Dynamic and Reversible Aggregation of the Human CAP Superfamily Member GAPR-1 in Protein Inclusions in *Saccharomyces cerevisiae*

Nafiseh Sirati [1], Blagovesta Popova [2], Martijn R. Molenaar [1†], Iris C. Verhoek [1], Gerhard H. Braus [2], Dora V. Kaloyanova [1] and J. Bernd Helms [1*]

*1 - **Division of Cell Biology,** Metabolism and Cancer, Faculty of Veterinary Medicine, Utrecht University, Utrecht, the Netherlands*
*2 - **Department of Molecular Microbiology and Genetics and Göttingen Center for Molecular Biosciences (GZMB),** Institute for Microbiology and Genetics, Universität Göttingen, Göttingen, Germany*

***Correspondence to J. Bernd Helms:** N.SiratiRoodbaraki@uu.nl (N. Sirati), J.B.Helms@uu.nl (J.B. Helms)*
https://doi.org/10.1016/j.jmb.2021.167162
Edited by Sheena E. Radford

Abstract

Many proteins that can assemble into higher order structures termed amyloids can also concentrate into cytoplasmic inclusions via liquid–liquid phase separation. Here, we study the assembly of human Golgi-Associated plant Pathogenesis Related protein 1 (GAPR-1), an amyloidogenic protein of the Cysteine-rich secretory proteins, Antigen 5, and Pathogenesis-related 1 proteins (CAP) protein superfamily, into cytosolic inclusions in *Saccharomyces cerevisiae*. Overexpression of GAPR-1-GFP results in the formation GAPR-1 oligomers and fluorescent inclusions in yeast cytosol. These cytosolic inclusions are dynamic and reversible organelles that gradually increase during time of overexpression and decrease after promoter shut-off. Inclusion formation is, however, a regulated process that is influenced by factors other than protein expression levels. We identified N-myristoylation of GAPR-1 as an important determinant at early stages of inclusion formation. In addition, mutations in the conserved metal-binding site (His54 and His103) enhanced inclusion formation, suggesting that these residues prevent uncontrolled protein sequestration. In agreement with this, we find that addition of Zn^{2+} metal ions enhances inclusion formation. Furthermore, Zn^{2+} reduces GAPR-1 protein degradation, which indicates stabilization of GAPR-1 in inclusions. We propose that the properties underlying both the amyloidogenic properties and the reversible sequestration of GAPR-1 into inclusions play a role in the biological function of GAPR-1 and other CAP family members.

Introduction

The Cysteine-rich secretory proteins, Antigen 5, and Pathogenesis-related 1 proteins (CAP) superfamily of proteins are widely spread in a variety of species and different kingdoms of life.[1] The highly conserved CAP domain characterises the CAP family members and forms a distinct core tertiary structure with a conserved metal-binding site. Golgi-Associated Plant Pathogenesis Related protein-1 (GAPR-1) is a unique member of the CAP superfamily, which branched off early in evolution and might well be the first mammalian CAP protein.[2,3] GAPR-1 is the only mammalian CAP protein that lacks a signal sequence and localises to the Golgi complex.[4] By retaining Beclin 1 at the Golgi complex, GAPR-1 functions as a negative regulator of autophagy.[5–7] GAPR-1 has a strong tendency to form homodimers and oligomers.[7,8] We showed that GAPR-1 can form amyloid-like fibrils and that this process is induced by the presence of negatively charged lipids or heparin and metal ions.[6,9,10]

These results show that different stimuli regulate amyloid-like oligomerisation of GAPR-1 *in vitro,* and we speculated that the amyloidogenic scaffold contributes to the regulation of GAPR-1 function *in vivo*.[9–11]

Structured cross β-sheet fibrils, known as amyloids, are highly resistant to degradation and are associated with more than 50 human diseases known as "amyloidoses".[12–14] Well known examples include neurodegenerative diseases like Alzheimer's and Parkinson's, where misfolding of Aβ, tau and α-synuclein is associated with progression of the disease.[15] The ability to form amyloid structures is, however, not limited to proteins causing pathology but seems to be a universal property of proteins.[16] Proteins and peptides forming amyloid-like oligomers with beneficial effects are often referred to as functional amyloids. The formation of these oligomers is tightly regulated and is characterised by their reversibility and plasticity.[11,13,17–19] Functional amyloids are implicated in a range of different physiological processes, including compartmentalisation, regulation of protein activity, storage and degradation.[20–25]

Recently it has become clear that proteins with amyloidogenic properties can cluster into cytoplasmic inclusions.[25–29] Evidence suggests that liquid–liquid phase separation (LLPS) underlies the formation of these cellular inclusions.[30–32] Although much remains to be elucidated about the driving forces and the nature of these biomolecular condensates, it has become clear that they represent distinct membraneless organelles in cells and that components can reversibly and dynamically associate with these structures. Transition from dynamic LLPS-mediated membraneless organelles to more static ones has been reported for several proteins associated with neurodegenerative disorders such as TDP-43, FUS, α-synuclein, tau and also functional amyloid-related proteins, including elastin, yeast prion-like protein Sup35, Rim4, and yeast pyruvate kinase Cdc19.[28,31,41,33–40] These observations suggest a link between the assemblies of membraneless organelles and amyloid-like protein behaviour in the cell.

Saccharomyces cerevisiae has been instrumental in the discovery and characterisation of pathological and functional amyloids.[42,43] Initially, so-called "humanised yeast" model systems were developed to study the oligomerisation properties of proteins involved in human amyloidosis like Aβ, tau and α-synuclein.[44–51] Expression of amyloidogenic proteins in yeast has several features in common such as the partial SDS-resistance of protein aggregates and the formation of inclusions or protein aggregates.[40,51,52] These properties have also been used to verify amyloid-like oligomerisation of sequence-predicted amyloid-prompt proteins in yeast model systems.[51,53–55] *Saccharomyces cerevisiae* does not express GAPR-1 and we use this model system to study human GAPR-1 amyloid-like oligomerisation *in vivo.* We show that GAPR-1 clusters into inclusions in yeast cytosol resembling GAPR-1 amyloid-like oligomerisation *in vitro*. We discuss the potential implications for the regulation of GAPR-1 function in autophagy.

Results

GAPR-1 clusters into fluorescent inclusions in yeast cytosol

To study the oligomerisation process of GAPR-1 *in vivo*, C-terminally tagged GAPR-1 with either GFP (GAPR-1-GFP) or mCherry (GAPR-1-mCherry) was expressed from 2μ plasmid in yeast under the control of the galactose-inducible promoter (*GAL1*). Overexpression of both GAPR-1-tagged variants did not affect yeast growth (Supplementary Figure 1(A)). Live-cell fluorescence microscopy was performed with GAPR-1-GFP and representative images were taken 3 h, 6 h and 24 h post-induction of protein expression. After 3 h, the majority of expressed protein was detected in the cytosol, with ~ 30% of all fluorescent cells displaying formation of cytosolic inclusions (Figure 1(A) and (B)). The number of inclusions significantly increased over time, affecting both the number of inclusion-positive cells (Figure 1(B)) and the number of inclusions per cell (Figure 1(C)). At 24 h post induction, about 94% of all cells contained multiple inclusions (Figure 1(B)) with an average of > 5 inclusions per cell (Figure 1(C)). The intracellular distribution of fluorescent inclusions also changed over time from being in close proximity to the plasma membrane at early stages and a more central cellular location at later stages. After 24 h, almost 60% of the yeast cells contained more than 6 inclusions per cell (Figure 1(C)). GAPR-1-GFP and GAPR-1-mCherry fusions displayed similar behaviour in live-cell fluorescence microscopy (Supplementary Figure 1(B)). To address whether the formation of inclusions is related to the level of protein expression, we assessed GAPR-1-GFP levels in cell lysates by Western blot analysis using an anti-GAPR-1 antibody. Although we observe a modest increase in expression levels between 3 h and 24 h (Figure 1(D)), it seems likely that additional factors affect the observed changes in inclusion formation (Figure 1(A)–(C)).

GAPR-1-GFP forms oligomeric structures in yeast

To investigate the oligomeric properties of GAPR-1-GFP after expression in yeast, we performed chemical cross-linking experiments using the amine-to-amine crosslinker BS^3. Expression of GAPR-1-GFP was induced for 6 h or 24 h, and the crosslinker was added for 30 min

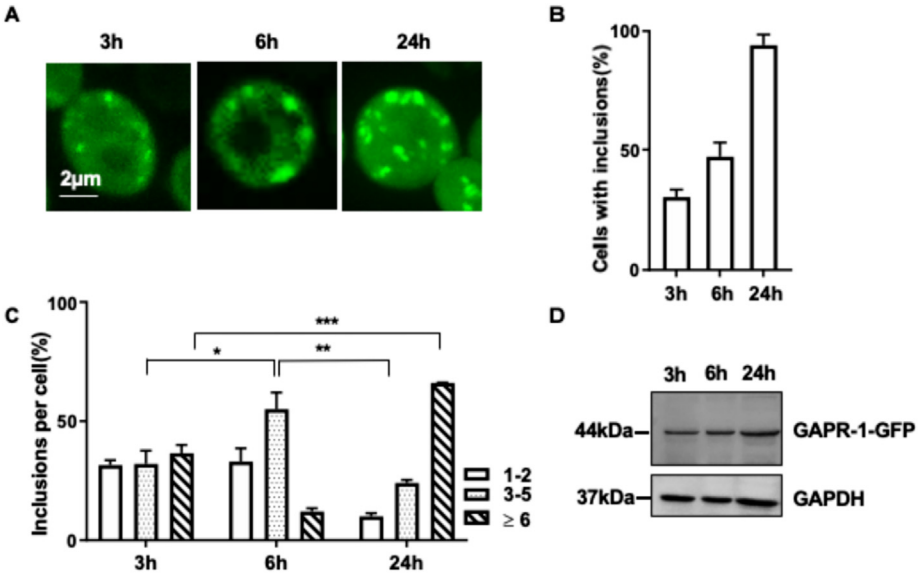

Figure 1. GAPR-1 clusters into fluorescent inclusions. (A) Representative live-cell fluorescence microscopy images of yeast cells expressing GAPR-1-GFP from 2μ plasmid (3 h, 6 h and 24 h after induction of protein expression); (B) Quantification of cells displaying GAPR-1-GFP inclusions. For each time point, the number of cells displaying cytoplasmic inclusions is quantified as described in Materials and Methods and presented as a percentage of the total number of the cells. Results are expressed as mean ± SD, n = 5; C) Quantification of the number of inclusions per cell. The number of inclusions per cell were categorised into three groups (1–2, 3–5 and ≥6 per cell). At least 100 cells were counted per experiment. Results are expressed as mean ± SD, n = 3. Significance of differences was calculated with two-tailed unpaired t-test ($^{*}p < 0.05$, $^{**}p < 0.01$ and $^{***}p < 0.001$); (D) WB analysis of GAPR-1-GFP expressing cells at 3 h, 6 h and 24 h post-induction. Equal amounts of yeast homogenate (20 μg total protein) were separated by SDS-PAGE and analysed by WB for the presence of GAPR-1-GFP and GAPDH (loading control).

at room temperature after mechanical disruption of the cells. Western blot analysis revealed that at early time points (6 h), the majority of overexpressed protein is in a monomeric state (Figure 2(A)). In contrast, at 24 h post-induction, higher-molecular weight species are observed in the BS^3-treated sample. A hallmark of amyloid-like oligomerisation *in vivo* is the partial protein resistance to solubilisation by SDS. To determine the amyloid-like characteristics of GAPR-1-GFP oligomerisation in yeast, a protein homogenate was separated into a detergent-soluble and detergent-insoluble fraction using a mild zwitterionic detergent. The detergent-insoluble fraction was then treated with 2% SDS and separated into a SDS-soluble and SDS-insoluble fraction. Western blot analysis showed that GAPR-1-GFP is partially soluble in mild detergent (Figure 2(B)). After subsequent SDS treatment of the detergent-insoluble fraction, about 50% of GAPR-1-GFP remained insoluble (Figure 2(B); Supplementary Figure 2(A)). Under these conditions, expression of GFP alone did not result in any detergent-insoluble material, even in the presence of only mild detergent (Figure 2(B)).

To obtain additional evidence for the amyloidogenic behaviour of GAPR-1-GFP, we performed Thioflavin T (ThT) fluorescence imaging of yeast cells. The ThT reagent becomes fluorescent upon intercalation into β-sheet structures of amyloid-like oligomers *in vivo* and *in vitro*.[56,57] Empty vector p423, GFP and GAPR-1-GFP expression was induced for 24 h and after staining of cells with ThT, total fluorescent intensity of cells was measured using 96 well plate reader. As it is shown in Figure 2(C), there was a significant increase in total ThT signal in the presence of GAPR-1-GFP comparing with empty vector and GFP. Live-cell microscopy of the ThT stained cells showed ThT labelling of GAPR-1-GFP and GAPR-1-mCherry inclusions (Figure 2(D)). The ThT signal was no due to spectral overlap with GFP as in the absence of ThT, no ThT-positive inclusions could be observed (Supplementary Figure 2(B)).

N-myristoylation of GAPR-1-GFP promotes inclusion formation

Membrane binding of numerous amyloidogenic proteins has been shown to promote amyloid nucleation and subsequent fibril formation *in vivo* and *in vitro*.[11,58–61] The membrane association of GAPR-1-GFP with yeast membranes was investigated by isopycnic density-gradient centrifugation of yeast homogenates obtained by mechanical homogenisation. GAPR-1-GFP was found mainly enriched in the high-density fractions 10–14

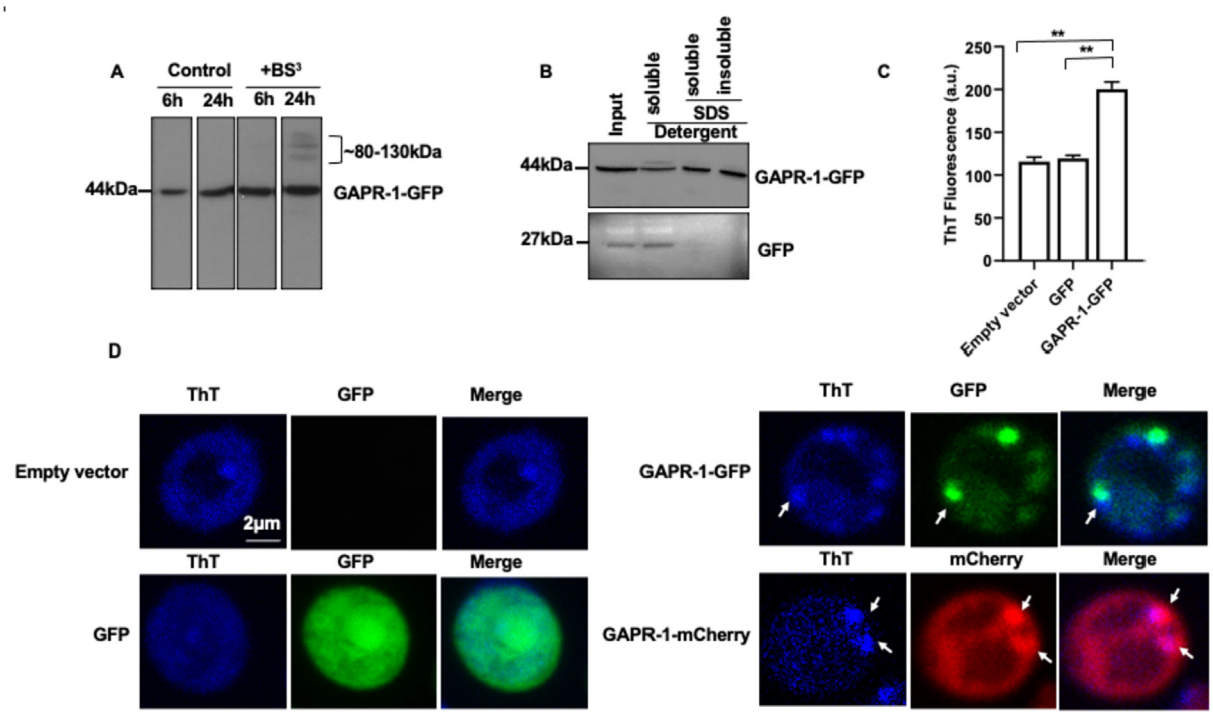

Figure 2. GAPR-1-GFP has oligomeric properties *in vivo*. A) Equal number of GAPR-1-GFP expressing cells were collected 6 h and 24 h post-induction of protein expression. Yeast homogenates (20 µg protein) were treated without (Control) or with 2.5 mM BS^3 (final concentration) for 30 min at room temperature. Proteins were separated by SDS-PAGE and analysed by WB using an anti-GAPR-1 antibody. High molecular weight species (12% of total, based on densitometric analysis, see Supplementary Figure 1(C)) with a mass of 80–130 kDa are indicated; (B) GAPR-1-GFP or GFP expression was induced for 24 h. Cells (10 OD_{600}) were collected, homogenised and homogenates were prepared using Y-PER™ reagent. After centrifugation, the pellet was treated with 2% SDS and separated into a SDS-soluble and SDS-insoluble fraction as described in Materials and Methods. The same volume (20 µl) of each sample was separated by SDS-PAGE and analysed by WB using an anti-GFP antibody; C) Total fluorescence intensity of Thioflavin T-stained cells after 24 h empty vector, GFP and GAPR-1-GFP expression. The results are expressed as the mean ± SEM, n = 4. Significance of differences was calculated with Welch t-test, corrected for multiple testing with Benjamini/Hochberg ($^{**}p < 0.01$); (D) Representative microscopic images of cells carrying empty vector, GFP, GAPR-1-GFP and GAPR-1-mCherry proteins after 24 h expression and stained with 5 µM Thioflavin T.

(37–41% sucrose density) (Figure 3(A)). About 20% of GAPR-1-GFP migrated with the low-density sucrose fractions 1–9 (25–36% sucrose density), suggesting that GAPR-1 is partially associated with membranes. When 1% Triton X-100 was added to the homogenate prior to the flotation, GAPR-1-GFP disappeared from the membrane fractions (1–9) (Figure 3(A)), supporting the conclusion that GAPR-GFP is partially associated with membranes. To assess the role of N-myristoylation in membrane association of GAPR-1-GFP and in the formation of protein inclusions, a GAPR-1 mutant lacking the N-terminal myristoylation consensus sequence (G2A; Δmyr-GAPR-1-GFP) was constructed by site-directed mutagenesis. Isopycnic density-gradient centrifugation showed that Δmyr-GAPR-1-GFP is found only in the high-density fractions (10–14), both in the presence and absence of 1% TX-100, suggesting that Δmyr-GAPR-1-GFP does not associate with membranes (Figure 3(B); Supplementary Figure 2(C)). The cellular distribution of Δmyr-GAPR-1-GFP was studied in time by live-cell fluorescence microscopy and representative images were taken at 3 h, 6 h and 24 h post-induction (Figure 3(C)). At early time points (3 h and 6 h), Δmyr-GAPR-1-GFP remained cytosolic and only after 24 h single inclusions were found in about 36% of the cells (Figure 3(D)). Under these conditions, the protein levels of Δmyr-GAPR-1-GFP are similar to the expression levels of GAPR-1-GFP (Supplementary Figure 2(D)) and they did not significantly change between the different time points (Figure 3(E)). These results indicate that the inclusion formation is subject to regulation by myristoylation of GAPR-1. To exclude the possibility that the myr-sequence itself plays a role in the aggregation process, independent of myristoylation, we overexpressed GAPR-1-GFP and Δmyr-GAPR-1-GFP in a yeast strain deficient in N-myristoyl transferase (ΔNMT1). The phenotype of both GAPR-1-GFP and Δmyr-GAPR-1-GFP in ΔNMT1 cells (Supplementary Figure 2(E))

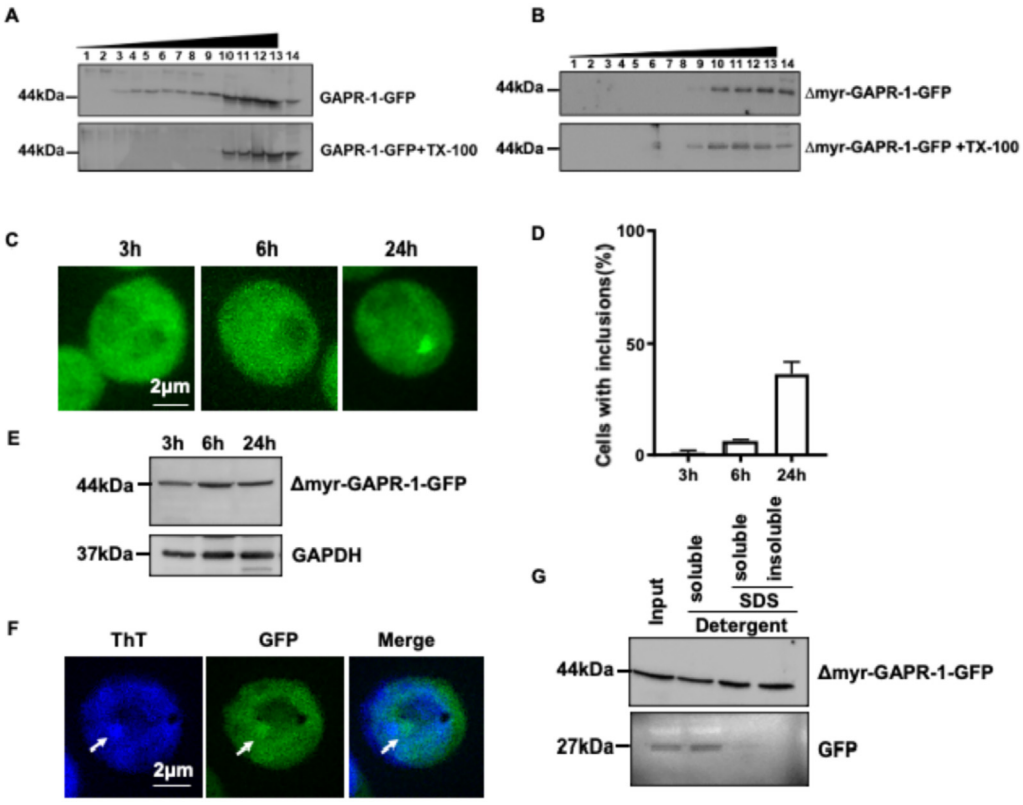

Figure 3. N-myristoylation of GAPR-1-GFP promotes formation of inclusions. (A) GAPR-1-GFP expressing cells (24 h) were collected, homogenised and treated without or with 1% TX-100 for 30 min on ice, followed by isopycnic density-gradient centrifugation. Fractions were collected from top to bottom and proteins in each fraction were separated by SDS-PAGE and analysed by WB using an anti-GAPR-1 antibody; (B) Δmyr-GAPR-1-GFP expressing cells (24 h) were collected and analysed by isopycnic density-gradient centrifugation and WB analysis as described for panel A; (C) Representative live-cell fluorescence microscopy images of cells after induction of Δmyr-GAPR-1-GFP expression (3 h, 6 h and 24 h); (D) Quantification of cells displaying Δmyr-GAPR-1-GFP fluorescent inclusions as described in Materials and Methods. Results are expressed as mean ± SD, n = 5; (E) Δmyr-GAPR-1-GFP expressing cells were collected at 3 h, 6 h and 24 h post-induction and total homogenates were prepared. Equal amounts of homogenate (20 μg protein) were separated by SDS-PAGE and analysed by WB for the presence of GAPR-1 and GAPDH (loading control); (F) Representative images of cells carrying Δmyr-GAPR-1-GFP protein after 24 h expression and stained with 5 μM Thioflavin T; (G) Δmyr-GAPR-1-GFP or GFP expression was induced for 24 h. Total homogenates were prepared using Y-PER™ reagent. After centrifugation, the pellet was treated with 2% SDS and separated into a SDS-soluble and SDS-insoluble fraction as described in Materials and Methods. The same volume (20 μl) of each sample was separated by SDS-PAGE and analysed by WB using an anti-GFP antibody.

resembled the phenotype of Δmyr-GAPR-1-GFP in wildtype yeast cells (Figure 3(C)). These results suggest that i) the myr-sequence itself does not play a role in the aggregation process, and ii) GAPR-1-GFP is myristoylated in wildtype yeast cells.

Interestingly, Δmyr-GAPR-1-GFP had similar amyloid-like characteristics as compared to GAPR-1-GFP based on its ThT staining (Figure 3(F), cf. Figure 2(D)) and SDS-insoluble characteristics (Figure 3(E), cf. Figure 2(B) and Supplementary Figure 2(A)). Despite these similar amyloid-like characteristics, Δmyr-GAPR-1-GFP is hampered in the formation of inclusions. Myristoylation likely accelerates the formation of protein inclusions by promoting membranes to function as a seeding platform for the assembly of GAPR-1 into oligomers and protein inclusions.

Metal-ions affect the formation of GAPR-1-GFP inclusions

We previously showed that zinc and copper ions induce GAPR-1 amyloid-like aggregation *in vitro* in the presence of heparin.[9,10] Therefore, we assessed the role of zinc in the formation of GAPR-1-GFP inclusions in yeast. Concentrations up to 10 mM $ZnCl_2$ are well tolerated by yeast cells (Supplementary Figure 3(A)), in agreement with results obtained by others.[62] We conducted live-cell fluorescence microscopy of cells in the absence and presence of 5 mM zinc ions and quantified the

number of inclusion forming cells at three time points (3 h, 6 h and 24 h). The percentage of fluorescent inclusions forming cells at 3 h post-induction almost doubled in the presence of zinc, reaching about 60% of the cells carrying fluorescent inclusions (Figure 4(A)). Representative images after 3 h post-induction are shown in Figure 4(B). The number of inclusions per cell also significantly changed at this early time point and showed a predominance of the "$\geq$ 6 inclusions pool" in comparison to the control cells (Figure 4(C)). These alterations were not triggered by different protein levels, as shown by Western blot analysis (Figure 4 (D)). Preliminary evidence shows similar effects in the presence of 2 mM Cu^{2+} (Supplementary Figure 3(B) and (C)). The data reveal that GAPR-1-GFP amyloid-like oligomerisation *in vivo* is influenced by zinc, similar to GAPR-1 amyloid aggregation *in vitro*.[9]

Zn^{2+} stabilises GAPR-1 protein inclusions

Next, we performed pulse-chase experiments to study the dynamics of GAPR-1 inclusions. To this end, GAPR1-GFP expression was first induced for 24 h in galactose-containing medium to generate GAPR-1 inclusions. Subsequently, the cells were shifted to glucose-containing medium to repress the promoter and to decrease the concentration of GAPR-1. Yeast cells were imaged at different time points after promoter shut-off and the percentage of cells with inclusions was determined. After promoter shut-off, both GAPR-1-GFP inclusions (Figure 5(B) and (E) control) and total GAPR-1 concentrations (Figure 5(B)) gradually decreased over time, which was accompanied by an increased cytosolic signal (Figure 5(A)). To investigate the dynamics of GAPR-1 protein inclusions in more detail, Fluorescence Recovery After Photo-bleaching (FRAP) analysis was performed on single fluorescent inclusions. After bleaching, GAPR-1-GFP inclusions were partially recovered in less than 2 min, indicating a dynamic association of GAPR-1-GFP with protein inclusions (Figure 5(C), top panel and Supplementary Movie 1). The fluorescence recovery in the presence of zinc ions was slightly faster as compared to the control cells (Figure 5 (C), bottom panel), suggesting that Zn^{2+} tweaks the equilibrium and stabilises GAPR-1 in inclusions. Indeed, the kinetics of protein degradation was much slower in the presence of Zn^{2+}, resulting in significantly higher GAPR-1-GFP levels at 6 h post-shut-off (Figure 5(D), left panel). Under these conditions, Zn^{2+} did not affect the degradation of GFP (Figure 5(D) (right panel), showing that the presence of Zn^{2+} does not affect the protein degradation machinery itself. These

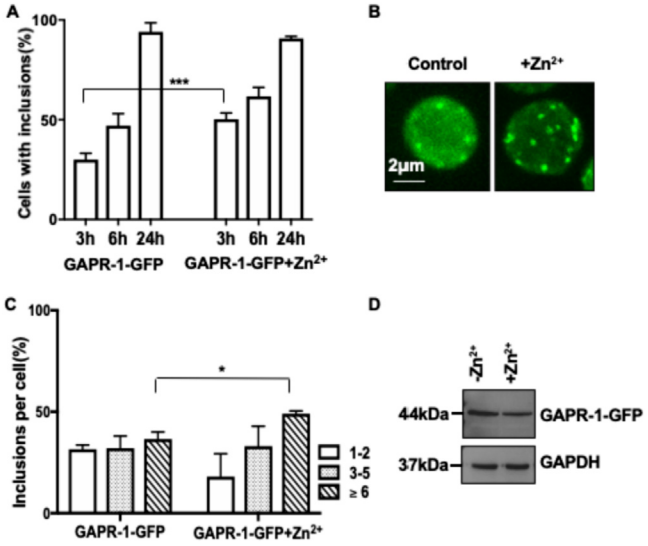

Figure 4. Metal-ions affect the formation of GAPR-1-GFP inclusions. Cells were incubated in the absence or presence of 5 mM Zn^{2+} for 3 h, 6 h, and 24 h after induction of GAPR-1-GFP expression. (A) Quantification of the percentage of cells displaying GAPR-1-GFP inclusions at 3 h, 6 h and 24 h post-induction. For each time point, the number of cells displaying cytoplasmic inclusions is quantified as described in Materials and Methods and presented as percentage of the total number of the cells. The results are expressed as mean ± SD, n = 5. Significance of differences was calculated with two-tailed unpaired t-test ($^{***}p < 0.001$); (B) Representative live-cell fluorescence microscopy images of cells, 3 h after expressing GAPR1-GFP in the absence or presence of 5 mM $ZnCl_2$; (C) Number of fluorescence inclusions per cell were quantified as described in Materials and Methods and plotted in three groups (1–2, 3–5 and $\geq$ 6 inclusions per cell). The results are expressed as mean ± SD, n = 3. Significance of differences was calculated with two-tailed unpaired t-test ($^{*}p < 0.05$); (D) WB analysis of homogenates (20 µg total protein) from GAPR-1-GFP expressing cells (3 h) in the absence or presence of 5 mM $ZnCl_2$ using an anti-GAPR-1 antibody. Anti-GAPDH antibody served as a loading control.

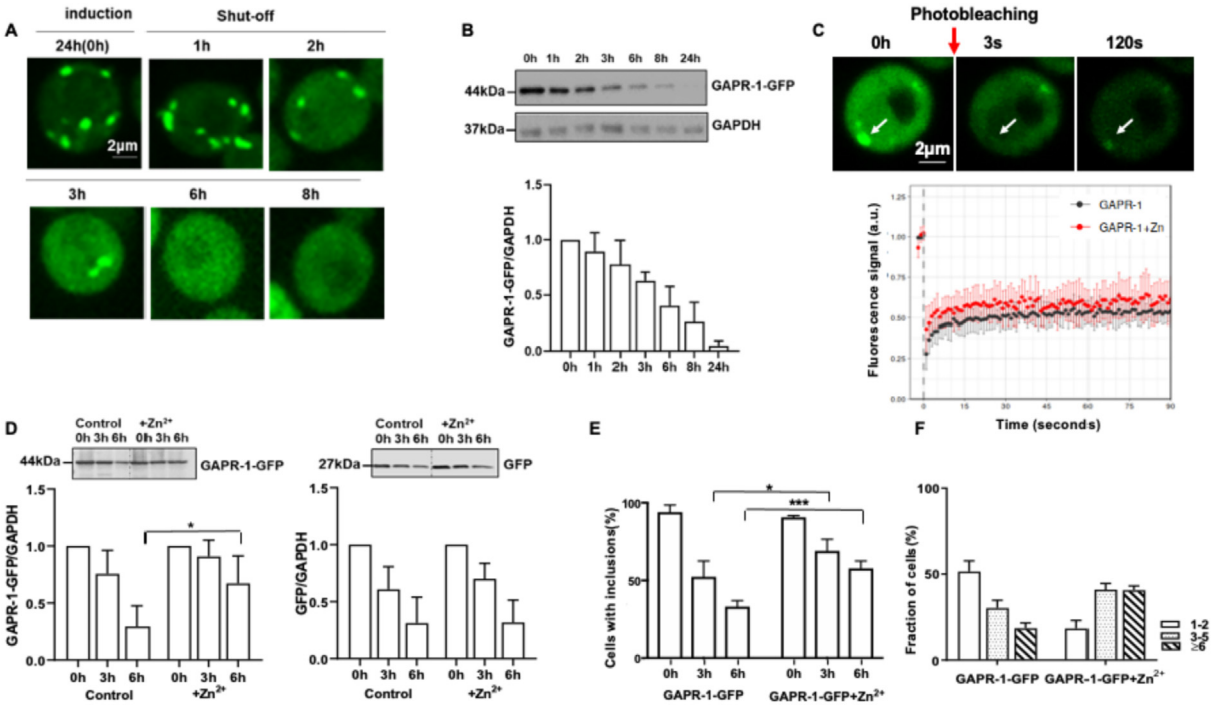

Figure 5. Zn^{2+} stabilises dynamic GAPR-1 protein inclusions. Pulse-chase analysis of protein expression. (A) Live-cell fluorescence microscopy of yeast cells expressing GAPR-1-GFP after 24 h induction (time point 0 h) and after promoter shut-off (1 h, 2 h, 3 h, 6 h and 8 h; (B) WB analysis of GAPR-1-GFP levels. Equal amounts of homogenates (20 ug total protein) were separated by SDS-PAGE and analysed by WB (top panel). Densitometric analysis of the immuno-detection of GAPR-1-GFP was determined relative to the intensity of GAPDH (bottom panel). Results are shown as one representative experiment from a total of three independent experiments; (C) Fluorescence Recovery After Photo-bleaching (FRAP) time lapse recording of a GAPR-1-GFP inclusion, and FRAP recovery curves of cells expressing GAPR-1-GFP in SC-galactose medium in the absence (control) and presence of 5 mM $ZnCl_2$, at the indicated time points. At least 15 inclusions in different cells were analysed. Each plot represents mean ± SD for each time point for all FRAP experiments; (D) Pulse-chase analysis in absence or presence of zinc ions. Protein expression of GAPR-1-GFP (left panel) or GFP (right panel) was induced for 24 h (time point 0 h), followed by promoter shut-off. Cells from 0 h, 3 h and at 6 h post-shut-off were collected and analysed by WB for the presence of GAPR-1-GFP and GAPDH (loading control). Densitometric analysis of the immuno-detection of GAPR-1-GFP and GFP were determined relative to the intensity of GAPDH ($^{*}p < 0.05$; n = 3); (E) Cells expressing GAPR-1-GFP from (B) were analysed by live-cell fluorescence microscopy and percentage of cells displaying fluorescence inclusions at 0 h, 3 h and 6 h post-shut-off GAPR-1-GFP expression in the absence or presence of Zn^{2+} were quantified in at least 200 cells. The results are expressed as means ± SD ($^{**}p < 0.01$, $^{***}p < 0.001$; n = 3). Differences between groups were statistically determined by using two-tailed unpaired t-test; (F) Quantification of the number of fluorescence inclusions per cell after 6 h promoter shut-off. Number of fluorescence inclusions per cell (from condition E) were categorised into three groups (1–2, 3–5 and ≥6 inclusions). At least 100 cells were counted per experiment. The results are expressed as mean ± SD, n = 3.

results indicate that Zn^{2+} reduces the protein dynamics and stabilises GAPR-1-GFP inclusions, thus preventing it from degradation. In agreement with this, we find that after promotor shut-off, the amount of fluorescent inclusions positive cells (Figure 5(E)) as well as the number of inclusions per cell (Figure 5(F)) is significantly increased in the presence of Zn^{2+}.

The conserved metal-binding pocket of GAPR-1 affects the formation of inclusions

Zinc-dependent amyloid-like oligomerisation of GAPR-1 *in vitro* requires two conserved histidine residues (H54 and H103).[9] To investigate the requirement of these histidines for the formation of GAPR-1 inclusions, GAPR-1-GFP mutants were constructed using site-directed mutagenesis (H54V, H103V, and H54V/H103V). Spotting assays revealed unperturbed growth of yeast cells expressing either of these mutants GAPR-1-GFP (Supplementary Figure 1(A)). The expressed histidine GAPR-1-GFP mutant proteins remained soluble after 100.000*g* centrifugation of yeast homogenates, indicating that the mutations did not disrupt protein folding (Supplementary Figure 4 (A)). Live fluorescence microscopy of yeast cells after expression of H103V and H54V/H103V

mutants showed that both mutants reached more than 80% inclusion-positive cells within 3 h (Figure 6(A) and (B); Control). These mutants did not show an additional sensitivity to zinc treatment anymore. Only the H54V mutant showed a moderate effect on inclusion formation in comparison to wild type GAPR-1-GFP and still showed a small but significant zinc effect on inclusion formation (Figure 6(A) and (B)). The steady-state protein levels of all expressed mutants were comparable in absence and presence of zinc (Figure 6(C)), showing that the observed phenotypes are not due to different levels of protein expression. To exclude a valine-specific effect on the phenotype of GAPR-1 histidine mutations, we found that the formation of protein inclusions and the sensitivity to zinc were similarly affected after replacement of histidine by alanine (H54A, H103A, and H54A/H103A) (Supplementary Figure 4(B)).

To explore whether myristoylation is still required for the enhanced inclusion formation in GAPR-1 His54V or His103V mutants, mutants lacking both the consensus sequence for myristoylation (Δmyr) and the metal-binding pocket (H54V/H103V) were created. As shown in Figure 6(D), all three mutants (ΔmyrH54V, ΔmyrH103V and ΔmyrH54V/H103V) remained predominantly soluble and insensitive to zinc treatment (Figure 6(D) and (F)) under conditions of similar levels of protein expression (Figure 6(E)). Thus, myristoylation remains a strong determinant for inclusion formation.

Discussion

GAPR-1 possesses amyloidogenic properties *in vitro* that are regulated by various factors such as negatively charged membranes and metal ions.[6,7,9,10] Here, we used the yeast *S. cerevisiae* to investigate the amyloid-like oligomerisation properties of GAPR-1-GFP *in vivo*. The involvement of the metal-binding site (His54 and His103) in the formation of GAPR-1 inclusions *in vivo* is strikingly similar to their involvement in Zn^{2+}-dependent GAPR-1 amyloid-like aggregation *in vitro*.[43]

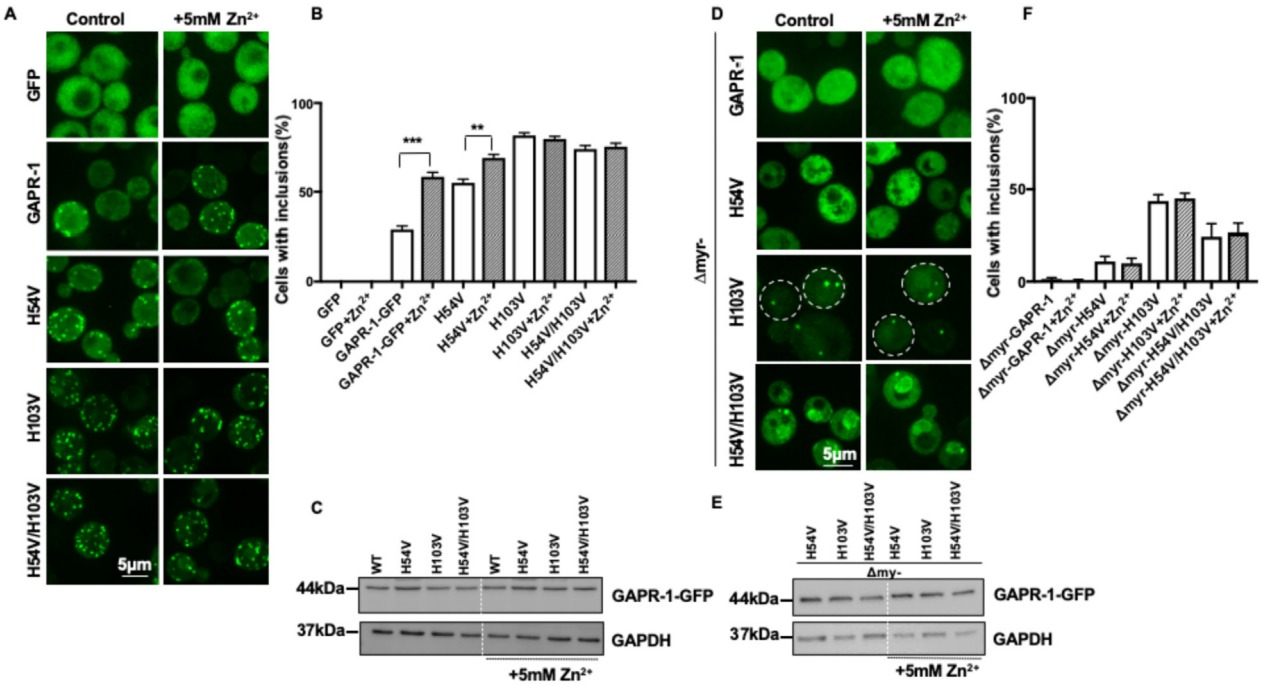

Figure 6. The conserved metal-binding pocket of GAPR-1 affects the formation of inclusions. Cells were transformed with GFP, GAPR-1-GFP, H54V, H103V and H54V/H103V (zinc ion binding sites-mutants) plasmids and protein expression was induced for 3 h in the absence and presence of 5 mM $ZnCl_2$. (A) Live-cell fluorescence microscopy images of representative cells; (B) Quantification of fluorescent inclusions in cells that were incubated as described for panel A as described in Materials and Methods; (C) Homogenates (20 μg protein) from each condition (A) were separated by SDS-PAGE and analysed by WB for the presence of GAPR-1-GFP and GAPDH (loading control); **(**D) Representative live-cell fluorescence microscopy images of cells expressing myristoylation mutants of GAPR-1 (Δmyr-GAPR-1, Δmyr-H54V, Δmyr-H103V and Δmyr-H54V/H103V). Protein expression was induced for 3 h in the absence or presence of 5 mM $ZnCl_2$; (E) Homogenates (20 μg protein) from each condition (D) was analysed by WB using an anti-GAPR-1 and anti-GAPDH (loading control) antibodies; **(**F) Quantification of cells displaying fluorescent inclusion as described in Materials and Methods. The results from B and F are expressed as mean ± SD, n = 3. Significance of differences was calculated with two-tailed unpaired t-test ($^{**}p < 0.01$; $^{***}p < 0.001$).

Hallmarks for the amyloidogenic behaviour of proteins overexpressed in yeast include SDS-resistance, ThT fluorescence, and formation of protein inclusions.[50,52–55,63–67] In the current study, we show that GAPR-1-GFP expression in yeast fulfils these criteria and results in the formation of SDS-resistant aggregates, elevated ThT fluorescence and formation of intracellular protein inclusions. In contrast to pathological amyloids[43,48,51,68–71] and similar to functional amyloids,[20,72,73] GAPR-1-GFP expression is not toxic for the cells. These observations support the concept that *in vivo* amyloid-like oligomerisation of GAPR-1 may have functional relevance.[11] GAPR-1 is bound to Golgi membranes and multiple factors may control its oligomeric status, such as the biophysical properties of the membranes that provide a specific surface catalysing structural changes (discussed below), specific negatively charged lipids interacting with GAPR-1,[4] and specific metal ions in the cytosol.[9,10] The oligomeric status of GAPR-1 could control GAPR-1 function and/or affect protein–protein interactions. GAPR-1 was identified as a negative regulator of the autophagic pathway. In agreement with our current findings, we recently suggested that GAPR-1 oligomerisation could be involved in the interaction with other components of the autophagic machinery and thus be essential for the GAPR-1 dependent autophagy regulation.[11]

Membranes can serve as catalytic sites that promote the (mis)folding and aggregation of bound amyloidogenic proteins.[74,75] In the past, we showed that GAPR-1 is stably bound to Golgi membranes by a mechanism which involves myristoylation of the N-terminus.[2] The myristoyl-group is, however, not essential for the formation of GAPR-1 amyloid-like fibrils *in vitro,* as recombinant non-myristoylated GAPR-1 aggregates to amyloid-like fibrils in the presence of a seeding platform.[6,9,10,76] In agreement with this, we now show that expression of Δmyr-GAPR-1-GFP in yeast cells also results in the formation of inclusions, albeit at much reduced efficiency as compared to GAPR-1-GFP. Myristoylation, together with relatively strong electrostatic interactions (GAPR-1 has an IP of 9.4), causes efficient interaction with membranes in mammalian cells.[77] In yeast cells, the partial distribution of overexpressed GAPR-1 between membranes and cytosol may be the result of suboptimal N-myristoylation due to high overexpression levels of GAPR-1-GFP or differences in substrate specificity of orthologous N-myristoyltransferases.[78]

Protein binding to membranes results in increased local concentrations and hence improved conditions for seed formation, which in turn accelerates amyloid-like oligomerisation and the formation of protein inclusions. Interestingly, there is no difference in SDS-solubility between Δmyr-GAPR-1-GFP (Figure 3) and GAPR-1-GFP (Figure 2), suggesting that the amyloidogenic properties are an intrinsic property of the GAPR-1 protein. In agreement with this, we previously reported that GAPR-1 possesses intrinsic amyloidogenic properties based on the finding that purified recombinant GAPR-1 binds to an A11 antibody that recognises the common fold of prefibrillar oligomers.[6] The difference in efficiency of inclusion formation between Δmyr-GAPR-1-GFP and GAPR-1-GFP strongly suggests that myristoylation catalyses the slowest step in inclusion formation, namely the clustering of GAPR-1 monomers and/or oligomers into protein inclusions. In addition, myristoylation acts upstream of the formation of protein inclusions as the effects of mutations to the metal-binding site on inclusion formation are largely prevented when myristoylation of GAPR-1 is prohibited (Figure 6). Of course, this does not exclude a potential role for myristoylation in the protein folding process itself, affecting the seeding process independent of membranes.

The process of *in vitro* amyloid-like aggregation of GAPR-1 requires small structural changes at early stages and large structural rearrangements for the formation of amyloid-like fibrils at later stages in the process.[9,10] The small structural changes can be induced by metal-ion-binding to the highly conserved metal-binding site that involves His54 and His103, resulting in enhanced sensitivity of proteases and the specific cleavage of a C-terminal fragment.[9,10] *In vivo*, we now confirm the sensitivity to zinc and show that the addition of zinc ions as well as a mutation of the GAPR-1 metal-binding site leads to an increase of inclusions (Figure 6). Together, these results suggest that small conformational changes in the GAPR-1 structure enhances protein clustering in inclusions and that inclusion formation resembles the early stages of GAPR-1 amyloid-like aggregation *in vitro* (Supplementary Figure 5). The enhanced accumulation of GAPR-1 in inclusions indicates stabilization of GAPR-1 in inclusions, resulting in reduced GAPR-1 dynamics into (FRAP) and from (protein degradation) inclusions (Figure 5). Stabilization of these structures that resemble early stages in amyloid-like aggregation formation are then predicted to inhibit amyloid-like fibril formation that occurs later during the process.[12,14,16] Indeed, a reduced amyloid-like fibril formation of GAPR-1 was observed upon mutations in the GAPR-1 metal-binding site.[9,10]

In summary, our results suggest a sequence of events that results in the formation of amyloid-like oligomers and fibrils summarised in Supplementary Figure 3: i) myristoylation acts early in the formation of protein inclusions as the effects of Zn^{2+} and mutations to the metal-binding site are largely prevented by mutations to the myristoylation site; ii) the metal-binding site is involved in the induction of small structural changes resulting in the formation of protein

inclusions; iii) large structural changes required for the formation of GAPR-1 amyloids occur at later stages and that have (so far) only been observed *in vitro* with non-myristoylated GAPR-1. GAPR-1 consists almost exclusively of a CAP domain without additional extensions.[1,2,8] We propose that metal-binding, in combination with a specific seeding platform, triggers oligomerisation to regulate the biological functions of various CAP family members. The yeast system may provide a beneficial model to elucidate the molecular mechanisms underlying protein oligomerisation of other CAP family members as well.

Materials and methods

Yeast strain and plasmids

Wild type yeast strain W303 was transformed by Frozen-EZ yeast kit from Zymo research (Zymo Research, Orange, CA, USA) with a high copy (2μ) plasmid p423 carrying different constructs with C-terminally-tagged GFP (Table 1). Yeast strains BY4741 (wild type and ΔNMT1-181 were obtained from EUROSCARF (Oberursel, Germany).

To construct P*GAL1*-GAPR-1-GFP and P*GAL1*-GAPR-1-mCherry fragments, GAPR-1, GFP and mCherry sequences (Supplementary Table 1 for primers) were amplified by PCR and were inserted into the plasmid p423, previously linearised at SmaI restriction site, by using Geneart® seamless cloning assembly kit (Invitrogen, California, USA). All mutants were constructed by using Phusion™ site-directed mutagenesis kit (Thermo Scientific, Massachusetts, USA). The primers are listed in Supplementary Table 1.

Yeast culture media

Cells were pre-grown overnight in synthetic complete medium lacking the corresponding marker (SC-His) and supplemented with either 2% glucose or 2% galactose at 30 °C with orbital agitation (200 rpm) for 18 h (overnight). The next day, optical density at 600 nm (OD_{600} nm) was measured, and the cells were placed in selective SC medium (OD_{600} = 0.1) supplemented with 2% galactose to induce protein expression. After 3, 6 and 24 h, cells were collected to obtain total cell homogenates or were observed under live-cell microscope Nikon Eclipse Ti-E (Nikon).

Spotting assay

All spotting assays were performed under the same conditions. Ten-fold serial dilutions starting with an equal number of cells (OD_{600} = 0.1) were performed in sterile water. Drops of 10 μl were then spotted on SC plates lacking the corresponding marker (SC-His) and supplemented with either 2% glucose or 2% galactose. Three independent experiments from fresh transformants were performed, followed by a 3 days incubation at 30 °C, after which the plates were scanned.

Fluorescence microscopy

Cells were visualised at different time points after induction (3 h, 6 h, and 24 h) using Nikon Eclipse Ti-E microscope (Nikon) equipped with the Perfect Focus System (Nikon) Nikon Apo TIRF 100x N.A. 1.49 oil objective (Nikon), a spinning disk-based confocal scanner unit (CSU-X1-A1, Yokogawa), and the ET-GFP filter set (49002, Chroma). For quantification, at least 300 cells were counted per condition and per experiment. For each condition, the number of cells displaying cytoplasmic inclusions were calculated relative to the total number of cells counted (with inclusions or cytoplasmic distribution). The number of inclusions per cell was determined by counting 100 cells and the inclusion positive cells were categorised in 3 groups: 1) 1–2 inclusions per cell, 2) 3–5 inclusions per cell, and 3) 6 or more than 6 inclusions per cell. At least three independent experiments with freshly transformed constructs were performed.

Table 1 Plasmids used in this study

Plasmid	Description	Source
p423-*GAL1*	2 μm*; HIS3; GAL1pr; CYC1term; AmpR*	79
pME3759	*p426-GAL1-GFP*	80
pNS 1000	*p423-GAL1-GAPR-1-GFP*	This study
pNS 1001	*p423-GAL1-*Δmyr *GAPR-1-GFP*	This study
pNS 1002	*p423-GAL1-H54V GAPR-1-GFP*	This study
pNS 1003	*p423-GAL1-H103V GAPR-1-GFP*	This study
pNS 1004	*p423-GAL1-H54V/H103V GAPR-1-GFP*	This study
pNS 1016	*p423-GAL1-*Δmyr *H54V GAPR-1-GFP*	This study
pNS 1017	*p423-GAL1-*Δmyr *H103V GAPR-1-GFP*	This study
pNS 1018	*p423-GAL1-*Δmyr *H54V/H103V GAPR-1-GFP*	This study

Protein extraction and Western blotting

10 OD units of cells were collected by centrifugation, washed with sterile water and lysed with 200 μl of Y-PER™ reagent (Thermo Scientific, Massachusetts, USA) containing fresh protease inhibitors (Aprotinin, Leupeptin, Pepstatin, PMSF) (Sigma Aldrich, St. Louis, USA). Lysed cells were incubated for 20 min at room temperature, followed by a 15 min centrifugation at 13,000 rpm. The supernatant containing total yeast homogenates were collected for further analysis. Yeast homogenates (20 μg protein) was mixed with Laemmli sample buffer, incubated for 5 min at 100 °C and separated by SDS-PAGE (12% polyacrylamide). Proteins were transferred onto 0.45 μm nitrocellulose membranes (Amersham Protran GE Healthcare) by Western blot at 90 V for 1 h. The presence of GAPR-1 was analysed using a rabbit polyclonal anti-GAPR-1 antibody.[2] A monoclonal anti-GAPDH antibody (Thermo Scientific, Massachusetts, USA) was used as a loading control. Peroxidase-conjugated goat anti-rabbit antibody (Nordic-Mubio, Susteren, The Netherlands) was used as a secondary antibody. Western blot analysis was performed using the SuperSignal™ reagents (Thermo Scientific, Massachusetts, USA) and ChemiDoc™ MP Imaging system (BioRad, Hercules, California, USA). For quantification of Western blots, pixel density values from TIFF files were analysed with Image Lab Software™. Sample density values were normalised to the corresponding GAPDH loading control. The statistical significance was calculated using two-tailed unpaired t-test.

SDS solubility test

10 OD unites of cells were collected after 24 h induction, homogenised and total protein homogenate was prepared using Y-PER™ reagent. 1/10 of the homogenate was collected as input. 9/10 of the sample was centrifuged at 100,000*g* for 30 min and the detergent-soluble supernatant was collected. The detergent-insoluble pellet was treated with 2% SDS (180 μl for 30 min at 4 °C) and separated by centrifugation (100,000*g* for 30 min) into a SDS-soluble and SDS-insoluble fraction. The same volume (20 μl) of each sample was separated by SDS-PAGE and analysed by Western blot using an anti-GFP antibody.

For the dot blot analyses, 50 μl (30 μg) of each sample was loaded directly onto 0.45 μm nitrocellulose membranes (Amersham Protran GE Healthcare) and analysed by an anti-GAPR-1 and anti-GFP antibodies.

Crosslinking assay

10 OD units of cells were collected at 6 and 24 h post-induction of GAPR-1-GFP protein expression. A homogenate was prepared by mechanical homogenisation with glass beads (0.25–0.5 mm, Carl Roth, Kalrsruhe, Germany). The homogenate (100 μg) was divided equally into two groups. Bis (sulfosuccinimidyl) suberate (BS^3) (Pierce Biotechnology, Rockford, IL, USA) was added in a 30-fold molar excess to the protein concentration to one of the groups and both groups were incubated for 30 min at room temperature. 0.5 M Tris pH 7.4 was added to quench the reaction. The proteins and cross-linked products were analysed by SDS-PAGE and Western blot.

Promoter shut-off study

Yeast cells containing GAPR-1-GFP constructs were cultured in SC selective medium supplemented with 2% raffinose overnight. The medium was changed to SC selective medium supplemented with 2% galactose to induce the GAPR-1-GFP expression for 24 h. The cells were pelleted, washed two times with water and shifted to SC medium supplemented with 2% glucose to shut-off the *GAL1* promoter.[80] Cells were visualised at different time points after promoter shut-off by fluorescence microscopy. The number of cells displaying GAPR-1-GFP inclusions were counted. Western blot analysis was performed as described above with homogenates prepared from cells collected at different time points after promoter shut-off.

Thioflavin T staining

Yeast cells were stained with Thioflavin T according to a protocol adapted from Johnson *et al.*[81] with minor modifications. Briefly, yeast cells were pre-grown overnight in SC-2% raffinose and then induced for 24 h in SC-2% galactose. Cells were harvested with a final OD of 0.25–1.0 and washed in 5 ml of PM [0.1 M KPO_4 (pH 7.5) and 1 mM $MgCl_2$], then re-suspended in PMST [0.1 M KPO_4 (pH 7.5), 1 mM $MgCl_2$, 1 M Sorbitol and 0.1% Tween 20] to a final OD of 10. To make spheroplasts, 100 μl of the cell suspension was incubated with 0.6 μl of 2-mercaptoethanol and 1 mg/ml Zymolyase (Zymo Research, Orange, CA, USA) for 15 min. Spheroplasted cells were washed once in PMST and re-suspended in 100 μl of PMST. Cells were then incubated 30 min at room temperature with 5 μM Thioflavin T (Sigma Aldrich, St. Louis, USA), followed by washing 3 times with PMST for 30 min. Cells were observed using Nikon Eclipse Ti-E microscope (Nikon) equipped with the Perfect Focus System (Nikon) Nikon Apo TIRF 100x N.A. 1.49 oil objective (Nikon) and a spinning disk-based confocal scanner unit (CSU-X1-A1, Yokogawa). GFP, mCherry and Thioflavin T signals were detected in GFP, mCherry and CFP channels, respectively. For measuring total ThT fluorescence intensity by a microplate reader, 100 μl of cells was pipetted into a 96-well plate

(black plastic plate with glass bottom, Greiner Bio-One, Frickenhausen, Germany). ThT (excitation at 380–420 nm, emission between 471 and 569, step size 5 nm) was measured with a microplate reader (CLARIOstar, BMG Labtech, Offenburg, Germany) using preset filter settings. Data were visualised and analysed in RStudio (v1.0.153, R v3.4.4) using R-package ggplot2 (v2.2.1). Total fluorescence per sample was calculated by integrating the areas under the curve between 480–510 nm (ThT).

Isopycnic sucrose density gradients and TX-100 treatment

Expressions of GAPR-1-GFP, Δmyr-GAPR-1-GFP and GFP (as control) were induced for 24 h in SC selective medium supplemented with 2% galactose. Cells were mechanically lysed with glass beads (0.25–0.5 mm, Carl Roth, Kalrsruhe, Germany). After centrifugation (13,000 rpm for 15 min at 4 °C), supernatants were collected and treated with or without 1% TX-100 for 30 min on ice. A sucrose gradient (37–35–29% sucrose in PBS buffer) was layered on top of 500 μl samples (adjusted to 37% sucrose and 50 μg total protein) in SW60-2 tubes (Beckman Coulter, Brea, California, USA). The samples were centrifuged at 60,000 rpm for 18 h in an ultracentrifuge. Fractions (350 μl) were collected from top to bottom of the gradients and were precipitated with Chloroform/Methanol (1/2). Samples were analysed by SDS-PAGE and Western blotting for the presence of GAPR-1 using specific antibodies (anti-GAPR-1 polyclonal antibody).

Fluorescence recovery after photo-bleaching (FRAP) analysis

Yeast cells harbouring GAPR-1-GFP were pre-grown overnight in SC selective medium containing 2% raffinose followed by 24 h induction in SC medium containing 2% galactose supplemented with or without 5 mM $ZnCl_2$ (Sigma Aldrich (St. Louis, USA). Cells were collected by centrifugation and re-suspended in PBS containing 0.5% low melting agarose on a microscope slide. FRAP experiments were performed using a Nikon A1Rsi microscope (Nikon) at room temperature. Images were acquired using a PlanApochromat 63x/1.4 gNA objective with frame size 256 × 256, pixel width 91 nm and pixel time 4.44 μs at intervals of 1 s with pinhole set to 1.5 Airy unit. In each FRAP experiment, a single focus at the central focal plane was bleached using the 488 nm laser line at 100% laser transmission on a circular region of interest (ROI) with a diameter of 8 pixels (0.7 μm radius) for 30 min. For imaging, the transmission of the 488 nm laser was set to 1% of the bleach intensity. Regions of interests (ROI) were defined for bleached spots, as well as for non-bleached spots. Mean fluorescence intensities for all ROIs were quantified over time using ImageJ (v1.50b). For every time point, signals from bleached spots were normalised to the signals from non-bleached spots to correct for fluorophore fading caused by image acquisition.

Statistical analysis

Data were analysed using GraphPad Prism 8 (San Diego, CA, USA) Software. The significance of differences was calculated using two-tailed unpaired t-test or Welch t-test. P-values lower than 0.05 were considered to indicate a significant difference.

CRediT authorship contribution statement

Nafiseh Sirati: Conceptualization, Methodology, Validation, Formal analysis, Investigation, Writing – original draft, Writing - review & editing, Visualization. **Blagovesta Popova:** Methodology, Validation, Formal analysis, Writing - review & editing. **Martijn R. Molenaar:** Validation, Formal analysis. **Iris C. Verhoek:** Validation. **Gerhard H. Braus:** Writing - review & editing, Funding acquisition. **Dora V. Kaloyanova:** Conceptualization, Writing – original draft, Writing - review & editing, Supervision. **J. Bernd Helms:** Conceptualization, Writing - review & editing, Supervision, Funding acquisition.

Acknowledgements

We thank Ruud Eerland and Ilse M. Lagerwaard for technical support, Richard Wubbolts and Ilya Grigoriev (Anna Akhmanova) for help with fluorescence microscopy. GB acknowledges the financial support of Deutsche Forschungsgemeinschaft (DFG: BR1502/18-1).

Declaration of Competing Interest

The authors declare that they have no known competing financial interests or personal relationships that could have appeared to influence the work reported in this paper.

Appendix A. Supplementary material

Supplementary data to this article can be found online at https://doi.org/10.1016/j.jmb.2021.167162.

Received 4 May 2021;
Accepted 12 July 2021;
Available online 21 July 2021

Keywords:
GLIPR-2;
condensates;
amyloids;
zinc;
myristoylation

† Present address: Structural and Computational Biology Unit, European Molecular Biology Laboratory, Heidelberg, Germany.

Abbreviations used:
GAPR-1, Golgi-Associated plant Pathogenesis Related protein 1; CAP, Cysteine-rich secretory proteins, Antigen 5, and Pathogenesis-related 1 proteins; GFP, Green fluorescent protein; Aβ, Amyloid β; TDP-43, TAR DNA-binding protein 43; FUS, Fused in Sarcoma; LLPS, Liquid-liquid phase separation; BS^3, Bis (sulfosuccinimidyl) suberate; ThT, Thioflavin T; SDS-PAGE, Sodium dodecyl sulphate-polyacrylamide gel electrophoresis; FRAP, Fluorescence Recovery After Photobleaching; GAPDH, Glyceraldehyde 3-phosphate dehydrogenase; SC, Synthetic Complete; WB, Western blot

References

1. Gibbs, G.M., Roelants, K., O'Bryan, M.K., (2008). The CAP superfamily: cysteine-rich secretory proteins, antigen 5, and pathogenesis-related 1 proteins—roles in reproduction, cancer, and immune defense. *Endocr. Rev.*, **29**, 865–897. https://doi.org/10.1210/er.2008-0032.
2. Eberle, H.B., Serrano, R.L., Füllekrug, J., Schlosser, A., Lehmann, W.D., Lottspeich, F., Kaloyanova, D., Wieland, F.T., et al., (2002). Identification and characterization of a novel human plant pathogenesis-related protein that localizes to lipid-enriched microdomains in the Golgi complex. *J. Cell Sci.*, **115**, 827–838 http://www.ncbi.nlm.nih.gov/pubmed/11865038.
3. Abraham, A., Chandler, D.E., (2017). Tracing the evolutionary history of the CAP superfamily of proteins using amino acid sequence homology and conservation of splice sites. *J. Mol. Evol.*, **85**, 137–157.
4. Van Galen, J., Van Balkom, B.W.M., Serrano, R.L., Kaloyanova, D., Eerland, R., Stüven, E., Helms, J.B., (2010). Binding of GAPR-1 to negatively charged phospholipid membranes: Unusual binding characteristics to phosphatidylinositol. *Mol. Membr. Biol.*, **27**, 81–91. https://doi.org/10.3109/09687680903507080.
5. Shoji-Kawata, S., Sumpter, R., Leveno, M., Campbell, G. R., Zou, Z., Kinch, L., Wilkins, A.D., Sun, Q., et al., (2013). Identification of a candidate therapeutic autophagy-inducing peptide. *Nature.*, **494**, 201–206. https://doi.org/10.1038/nature11866.
6. Olrichs, N.K., Mahalka, A.K., Kaloyanova, D., Kinnunen, P. K., Bernd Helms, J., (2014). Golgi-Associated plant Pathogenesis Related protein 1 (GAPR-1) forms amyloid-like fibrils by interaction with acidic phospholipids and inhibits Aβ aggregation. *Amyloid.*, **21**, 88–96. https://doi.org/10.3109/13506129.2014.882304.
7. Van Galen, J., Olrichs, N.K., Schouten, A., Serrano, R.L., Nolte-'t Hoen, E.N.M., Eerland, R., Kaloyanova, D., Gros, P., et al., (2012). Interaction of GAPR-1 with lipid bilayers is regulated by alternative homodimerization. *Biochim. Biophys. Acta - Biomembr.*, **1818**, 2175–2183. https://doi.org/10.1016/j.bbamem.2012.04.016.
8. Serrano, R.L., Kuhn, A., Hendricks, A., Helms, J.B., Sinning, I., Groves, M.R., (2004). Structural analysis of the human Golgi-associated plant pathogenesis related protein GAPR-1 implicates dimerization as a regulatory mechanism. *J. Mol. Biol.*, **339**, 173–183. https://doi.org/10.1016/j.jmb.2004.03.015.
9. Sheng, J., Olrichs, N.K., Geerts, W.J., Li, X., Rehman, A. U., Gadella, B.M., Kaloyanova, D.V., Helms, J.B., (2019). Zinc binding regulates amyloid-like aggregation of GAPR-1. *Biosci. Rep.*, **39** https://doi.org/10.1042/BSR20182345.
10. Sheng, J., Olrichs, N.K., Geerts, W.J., Kaloyanova, D.V., Helms, J.B., (2019). Metal ions and redox balance regulate distinct amyloid-like aggregation pathways of GAPR-1. *Sci. Rep.*, **9**, 15048. https://doi.org/10.1038/s41598-019-51232-7.
11. Sheng, J., Olrichs, N.K., Gadella, B.M., Kaloyanova, D.V., Helms, J.B., (2020). Regulation of functional protein aggregation by multiple factors: implications for the amyloidogenic behavior of the CAP superfamily proteins. *Int. J. Mol. Sci.*, **21**, 6530. https://doi.org/10.3390/ijms21186530.
12. Tyedmers, J., Mogk, A., Bukau, B., (2010). Cellular strategies for controlling protein aggregation. *Nature Rev. Mol. Cell Biol.*, **11**, 777–788. https://doi.org/10.1038/nrm2993.
13. Chiti, F., Dobson, C.M., (2006). Protein misfolding, functional amyloid, and human disease. *Annu. Rev. Biochem.*, **75**, 333–366. https://doi.org/10.1146/annurev.biochem.75.101304.123901.
14. Chiti, F., Dobson, C.M., (2017). Protein misfolding, amyloid formation, and human disease: a summary of progress over the last decade. *Annu. Rev. Biochem.*, **86**, 27–68. https://doi.org/10.1146/annurev-biochem-061516-045115.
15. Iadanza, M.G., Jackson, M.P., Hewitt, E.W., Ranson, N.A., Radford, S.E., (2018). A new era for understanding amyloid structures and disease. *Nature Rev. Mol. Cell Biol.*, **19**, 755–773. https://doi.org/10.1038/s41580-018-0060-8.
16. Knowles, T.P.J., Vendruscolo, M., Dobson, C.M., (2014). The amyloid state and its association with protein misfolding diseases. *Nature Rev. Mol. Cell Biol.*, **15**, 384–396. https://doi.org/10.1038/nrm3810.
17. Chuang, E., Hori, A.M., Hesketh, C.D., Shorter, J., (2018). Amyloid assembly and disassembly. *J. Cell Sci.*, **131**, 1–18.
18. Otzen, D., Riek, R., (2019). Functional amyloids. *Cold Spring Harb. Perspect. Biol.*, **11**, https://doi.org/10.1101/cshperspect.a033860 a033860.
19. Fowler, D.M., Koulov, A.V., Balch, W.E., Kelly, J.W., (2007). Functional amyloid – from bacteria to humans. *Trends Biochem. Sci.*, **32**, 217–224. https://doi.org/10.1016/j.tibs.2007.03.003.
20. Ulamec, S.M., Radford, S.E., (2020). Spot the difference: function versus toxicity in amyloid fibrils. *Trends Biochem. Sci.*, **45**, 635–636. https://doi.org/10.1016/j.tibs.2020.04.007.
21. Saad, S., Cereghetti, G., Feng, Y., Picotti, P., Peter, M., Dechant, R., (2017). Reversible protein aggregation is a protective mechanism to ensure cell cycle restart after stress. *Nature Cell Biol.*, **19**, 1202–1213. https://doi.org/10.1038/ncb3600.

22. Audas, T.E., Audas, D.E., Jacob, M.D., Ho, J.J.D., Khacho, M., Wang, M., Perera, J.K., Gardiner, C., et al., (2016). Adaptation to Stressors by Systemic Protein Amyloidogenesis. *Dev. Cell.*, **39**, 155–168. https://doi.org/10.1016/j.devcel.2016.09.002.
23. Maji, S.K., Perrin, M.H., Sawaya, M.R., Jessberger, S., Vadodaria, K., Rissman, R.A., Singru, P.S., Nilsson, K.P. R., et al., (2009). Functional amyloids as natural storage of peptide hormones in pituitary secretory granules. *Science (80-.)*, **325**, 328–332. https://doi.org/10.1126/science.1173155.
24. Hewetson, A., Do, H.Q., Myers, C., Muthusubramanian, A., Sutton, R.B., Wylie, B.J., Cornwall, G.A., (2017). Functional amyloids in reproduction. *Biomolecules.*, **7**, 46. https://doi.org/10.3390/biom7030046.
25. Rubel, M.S., Fedotov, S.A., Grizel, A.V., Sopova, J.V., Malikova, O.A., Chernoff, Y.O., Rubel, A.A., (2020). Functional mammalian amyloids and amyloid-like proteins. *Life*, **10**, 156. https://doi.org/10.3390/life10090156.
26. Patel, A., Lee, H.O., Jawerth, L., Maharana, S., Jahnel, M., Hein, M.Y., Stoynov, S., Mahamid, J., et al., (2015). A liquid-to-solid phase transition of the ALS protein FUS accelerated by disease mutation. *Cell*, **162**, 1066–1077. https://doi.org/10.1016/j.cell.2015.07.047.
27. Amen, T., Kaganovich, D., (2015). Dynamic droplets: the role of cytoplasmic inclusions in stress, function, and disease. *Cell. Mol. Life Sci.*, **72**, 401–415. https://doi.org/10.1007/s00018-014-1740-y.
28. Zbinden, A., Pérez-Berlanga, M., De Rossi, P., Polymenidou, M., (2020). Phase separation and neurodegenerative diseases: a disturbance in the force. *Dev. Cell.*, **55**, 45–68. https://doi.org/10.1016/j.devcel.2020.09.014.
29. Elbaum-Garfinkle, S., (2019). Matter over mind: liquid phase separation and neurodegeneration. *J. Biol. Chem.*, **294**, 7160–7168. https://doi.org/10.1074/jbc.REV118.001188.
30. Gomes, E., Shorter, J., (2019). The molecular language of membraneless organelles. *J. Biol. Chem.*, **294**, 7115–7127. https://doi.org/10.1074/jbc.TM118.001192.
31. Alberti, S., Gladfelter, A., Mittag, T., (2019). Considerations and challenges in studying liquid-liquid phase separation and biomolecular condensates. *Cell*, **176**, 419–434. https://doi.org/10.1016/j.cell.2018.12.035.
32. Alberti, S., Hyman, A.A., (2021). Biomolecular condensates at the nexus of cellular stress, protein aggregation disease and ageing. *Nature Rev. Mol. Cell Biol.*, **22**, 196–213. https://doi.org/10.1038/s41580-020-00326-6.
33. Franzmann, T.M., Jahnel, M., Pozniakovsky, A., Mahamid, J., Holehouse, A.S., Nüske, E., Richter, D., Baumeister, W., et al., (2018). Phase separation of a yeast prion protein promotes cellular fitness. *Science (80-.).*, **359**, eaao5654. https://doi.org/10.1126/science.aao5654.
34. Sanchez de Groot, N., Torrent Burgas, M., Ravarani, C.N., Trusina, A., Ventura, S., Babu, M.M., (2019). The fitness cost and benefit of phase-separated protein deposits. *Mol. Syst. Biol.*, **15** https://doi.org/10.15252/msb.20178075.
35. Alberti, S., Hyman, A.A., (2016). Are aberrant phase transitions a driver of cellular aging? *BioEssays*, **38**, 959–968. https://doi.org/10.1002/bies.201600042.
36. Boeynaems, S., Alberti, S., Fawzi, N.L., Mittag, T., Polymenidou, M., Rousseau, F., Schymkowitz, J., Shorter, et al., (2018). Protein phase separation: a new phase in cell biology. *Trends Cell Biol.*, **28**, 420–435. https://doi.org/10.1016/j.tcb.2018.02.004.
37. Alberti, S., Carra, S., (2018). Quality control of membraneless organelles. *J. Mol. Biol.*, **430**, 4711–4729. https://doi.org/10.1016/j.jmb.2018.05.013.
38. Ke, P.C., Zhou, R., Serpell, L.C., Riek, R., Knowles, T.P.J., Lashuel, H.A., Gazit, E., Hamley, I.W., et al., (2020). Half a century of amyloids: past, present and future. *Chem. Soc. Rev.*, **49**, 5473–5509. https://doi.org/10.1039/C9CS00199A.
39. Muiznieks, L.D., Sharpe, S., Pomès, R., Keeley, F.W., (2018). Role of liquid-liquid phase separation in assembly of elastin and other extracellular matrix proteins. *J. Mol. Biol.*, **430**, 4741–4753. https://doi.org/10.1016/j.jmb.2018.06.010.
40. Berchowitz, L.E., Kabachinski, G., Walker, M.R., Carlile, T. M., Gilbert, W.V., Schwartz, T.U., Amon, A., (2015). Regulated formation of an amyloid-like translational repressor governs gametogenesis. *Cell*, **163**, 406–418. https://doi.org/10.1016/j.cell.2015.08.060.
41. Balistreri, A., Goetzler, E., Chapman, M., (2020). Functional amyloids are the rule rather than the exception in cellular biology. *Microorganisms*, **8**, 1951. https://doi.org/10.3390/microorganisms8121951.
42. Khurana, V., Lindquist, S., (2010). Modelling neurodegeneration in Saccharomyces cerevisiae: why cook with baker's yeast? *Nature Rev. Neurosci.*, **11**, 436–449. https://doi.org/10.1038/nrn2809.
43. Tardiff, D.F., Khurana, V., Chung, C.Y., Lindquist, S., (2014). From yeast to patient neurons and back again: powerful new discovery platforms. *Mov. Disord.*, **29**, 1231–1240. https://doi.org/10.1002/mds.25989.
44. Fruhmann, G., Seynnaeve, D., Zheng, J., Ven, K., Molenberghs, S., Wilms, T., Liu, B., Winderickx, J., et al., (2017). Yeast buddies helping to unravel the complexity of neurodegenerative disorders. *Mech. Ageing Dev.*, **161**, 288–305. https://doi.org/10.1016/j.mad.2016.05.002.
45. McGurk, L., Bonini, N.M., (2011). Yeast informs Alzheimer's disease. *Science (80-.)*, **334**, 1212–1213. https://doi.org/10.1126/science.1216073.
46. Porzoor, A., Macreadie, I.G., (2013). Application of yeast to study the tau and amyloid-β abnormalities of Alzheimer's disease. *J. Alzheimer's Dis.*, **35**, 217–225. https://doi.org/10.3233/JAD-122035.
47. Outeiro, T.F., (2003). Yeast cells provide insight into alpha-synuclein biology and pathobiology. *Science (80-.)*, **302**, 1772–1775. https://doi.org/10.1126/science.1090439.
48. Brás, I.C., Popova, B., Braus, G.H., & Outeiro, T.F. (2019). Yeast-Based Screens to Target Alpha-Synuclein Toxicity, pp. 145–156. https://doi.org/10.1007/978-1-4939-9124-2_12.
49. Tenreiro, S., Munder, M.C., Alberti, S., Outeiro, T.F., (2013). Harnessing the power of yeast to unravel the molecular basis of neurodegeneration. *J. Neurochem.*, **127**, 438–452. https://doi.org/10.1111/jnc.12271.
50. Tenreiro, S., Reimão-Pinto, M.M., Antas, P., Rino, J., Wawrzycka, D., Macedo, D., Rosado-Ramos, R., Amen, T., et al., (2014). Phosphorylation modulates clearance of alpha-synuclein inclusions in a yeast model of Parkinson's disease. *PLoS Genet.*, **10**, https://doi.org/10.1371/journal.pgen.1004302 e1004302.
51. Popova, B., Kleinknecht, A., Arendarski, P., Mischke, J., Wang, D., Braus, G.H., (2018). Sumoylation protects

against β-synuclein toxicity in yeast. *Front. Mol. Neurosci.*, **11** https://doi.org/10.3389/fnmol.2018.00094.
52. Alberti, S., Halfmann, R., & Lindquist, S. (2010). Biochemical, Cell Biological, and Genetic Assays to Analyze Amyloid and Prion Aggregation in Yeast, pp. 709–734. https://doi.org/10.1016/S0076-6879(10)70030-6.
53. Laor, D., Sade, D., Shaham-Niv, S., Zaguri, D., Gartner, M., Basavalingappa, V., Raveh, A., Pichinuk, E., Engel, H., Iwasaki, K., Yamamoto, T., Noothalapati, H., Gazit, E., (2019). Fibril formation and therapeutic targeting of amyloid-like structures in a yeast model of adenine accumulation. *Nature Commun.*, **10**, 62. https://doi.org/10.1038/s41467-018-07966-5.
54. Rencus-Lazar, S., DeRowe, Y., Adsi, H., Gazit, E., Laor, D., (2019). Yeast models for the study of amyloid-associated disorders and development of future therapy. *Front. Mol. Biosci.*, **6** https://doi.org/10.3389/fmolb.2019.00015.
55. Cereghetti, G., Saad, S., Dechant, R., Peter, M., (2018). Reversible, functional amyloids: towards an understanding of their regulation in yeast and humans. *Cell Cycle*, **17**, 1545–1558. https://doi.org/10.1080/15384101.2018.1480220.
56. Biancalana, M., Koide, S., (1804). Molecular mechanism of Thioflavin-T binding to amyloid fibrils. *Biochim. Biophys. Acta - Proteins Proteom.*, **2010**, 1405–1412. https://doi.org/10.1016/j.bbapap.2010.04.001.
57. Ohhashi, Y., Yamaguchi, Y., Kurahashi, H., Kamatari, Y. O., Sugiyama, S., Uluca, B., Piechatzek, T., Komi, Y., et al., (2018). Molecular basis for diversification of yeast prion strain conformation. *Proc. Natl. Acad. Sci.*, **115**, 2389–2394. https://doi.org/10.1073/pnas.1715483115.
58. Fanni, A.M., Vander Zanden, C.M., Majewska, P.V., Majewski, J., Chi, E.Y., (2019). Membrane-mediated fibrillation and toxicity of the tau hexapeptide PHF6. *J. Biol. Chem.*, **294**, 15304–15317. https://doi.org/10.1074/jbc.RA119.010003.
59. Khondker, A., Alsop, R.J., Rheinstädter, M.C., (2017). Membrane-accelerated Amyloid-β aggregation and formation of cross-β sheets. *Membranes (Basel)*, **7** https://doi.org/10.3390/membranes7030049.
60. McLaurin, J., Franklin, T., Zhang, X., Deng, J., Fraser, P. E., (1999). Interactions of Alzheimer amyloid-β peptides with glycosaminoglycans. *Eur. J. Biochem.*, **266**, 1101–1110. https://doi.org/10.1046/j.1432-1327.1999.00957.x.
61. Mehra, S., Ghosh, D., Kumar, R., Mondal, M., Gadhe, L.G., Das, S., Anoop, A., Jha, N.N., et al., (2018). Glycosaminoglycans have variable effects on -synuclein aggregation and differentially affect the activities of the resulting amyloid fibrils. *J. Biol. Chem.*, **293**, 12975–12991. https://doi.org/10.1074/jbc.RA118.004267.
62. Ishii, A., Kurokawa, K., Hotta, M., Yoshizaki, S., Kurita, M., Koyama, A., Nakano, A., Kimura, Y., (2019). Role of Atg8 in the regulation of vacuolar membrane invagination. *Sci. Rep.*, **9**, 14828. https://doi.org/10.1038/s41598-019-51254-1.
63. Chernova, T.A., Chernoff, Y.O., Wilkinson, K.D., (2019). Yeast models for amyloids and prions: environmental modulation and drug discovery. *Molecules*, **24**, 3388. https://doi.org/10.3390/molecules24183388.
64. Wickner, R.B., Kryndushkin, D., Shewmaker, F., McGlinchey, R., & Edskes, H.K. (2018). Study of Amyloids Using Yeast, pp. 313–339. https://doi.org/10.1007/978-1-4939-7816-8_19.
65. Monahan, Z.T., Rhoads, S.N., Yee, D.S., Shewmaker, F. P., (2018). Yeast models of prion-like proteins that cause amyotrophic lateral sclerosis reveal pathogenic mechanisms. *Front. Mol. Neurosci.*, **11** https://doi.org/10.3389/fnmol.2018.00453.
66. Sergeeva, A.V., Sopova, J.V., Belashova, T.A., Siniukova, V.A., Chirinskaite, A.V., Galkin, A.P., Zadorsky, S.P., (2019). Amyloid properties of the yeast cell wall protein Toh1 and its interaction with prion proteins Rnq1 and Sup35. *Prion.*, **13**, 21–32. https://doi.org/10.1080/19336896.2018.1558763.
67. Kryndushkin, D., Pripuzova, N., Burnett, B.G., Shewmaker, F., (2013). Non-targeted identification of prions and amyloid-forming proteins from yeast and mammalian cells. *J. Biol. Chem.*, **288**, 27100–27111. https://doi.org/10.1074/jbc.M113.485359.
68. Lindström, M., Liu, B., (2018). Yeast as a model to unravel mechanisms behind FUS toxicity in amyotrophic lateral sclerosis. *Front. Mol. Neurosci.*, **11** https://doi.org/10.3389/fnmol.2018.00218.
69. Chernoff, Y.O., Grizel, A.V., Rubel, A.A., Zelinsky, A.A., Chandramowlishwaran, P., & Chernova, T.A. (2020). Application of yeast to studying amyloid and prion diseases, pp. 293–380. https://doi.org/10.1016/bs.adgen.2020.01.002.
70. Villar-Piqué, A., Ventura, S., (1833). Protein aggregation propensity is a crucial determinant of intracellular inclusion formation and quality control degradation. *Biochim. Biophys. Acta - Mol. Cell Res.*, **2013**, 2714–2724. https://doi.org/10.1016/j.bbamcr.2013.06.023.
71. Sampaio-Marques, B., Guedes, A., Vasilevskiy, I., Gonçalves, S., Outeiro, T.F., Winderickx, J., Burhans, W. C., Ludovico, P., (2019). α-Synuclein toxicity in yeast and human cells is caused by cell cycle re-entry and autophagy degradation of ribonucleotide reductase 1. *Aging Cell*, **18** https://doi.org/10.1111/acel.12922.
72. Rueda, F., Gasser, B., Sánchez-Chardi, A., Roldán, M., Villegas, S., Puxbaum, V., Ferrer-Miralles, N., Unzueta, U., et al., (2016). Functional inclusion bodies produced in the yeast Pichia pastoris. *Microb. Cell Fact.*, **15**, 166. https://doi.org/10.1186/s12934-016-0565-9.
73. Jackson, M., Hewitt, E., (2017). Why are functional amyloids non-toxic in humans? *Biomolecules*, **7**, 71. https://doi.org/10.3390/biom7040071.
74. Butterfield, S.M., Lashuel, H.A., (2010). Amyloidogenic protein-membrane interactions: mechanistic insight from model systems. *Angew. Chemie Int. Ed.*, **49**, 5628–5654. https://doi.org/10.1002/anie.200906670.
75. Musteikytė, G., Jayaram, A.K., Xu, C.K., Vendruscolo, M., Krainer, G., Knowles, T.P.J., (2021). Interactions of α-synuclein oligomers with lipid membranes. *Biochim. Biophys. Acta - Biomembr.*, **1863**, https://doi.org/10.1016/j.bbamem.2020.183536 183536.
76. Olrichs, N.K., Bernd Helms, J., (2016). Novel insights into the function of the conserved domain of the CAP superfamily of proteins. *AIMS Biophys.*, **3**, 232–246. https://doi.org/10.3934/biophy.2016.2.232.
77. Resh, M.D., (1999). Fatty acylation of proteins: new insights into membrane targeting of myristoylated and palmitoylated proteins. *Biochim. Biophys. Acta - Mol. Cell Res.*, **1451**, 1–16. https://doi.org/10.1016/S0167-4889(99)00075-0.
78. Farazi, T.A., Waksman, G., Gordon, J.I., (2001). The biology and enzymology of protein N-myristoylation. *J. Biol.*

Chem., **276**, 39501–39504. https://doi.org/10.1074/jbc.R100042200.

79. Mumberg, D., Muller, R., Funk, M., (1994). Regulatable promoters of Saccharomyces cerevisiae: comparison of transcriptional activity and their use for heterologous expression. *Nucleic Acids Res.*, **22**, 5767–5768. https://doi.org/10.1093/nar/22.25.5767.
80. Petroi, D., Popova, B., Taheri-Talesh, N., Irniger, S., Shahpasandzadeh, H., Zweckstetter, M., Outeiro, T.F., Braus, G.H., (2012). Aggregate clearance of α-synuclein in Saccharomyces cerevisiae depends more on autophagosome and vacuole function than on the proteasome. *J. Biol. Chem.*, **287**, 27567–27579. https://doi.org/10.1074/jbc.M112.361865.
81. Johnson, B.S., McCaffery, J.M., Lindquist, S., Gitler, A.D., (2008). A yeast TDP-43 proteinopathy model: Exploring the molecular determinants of TDP-43 aggregation and cellular toxicity. *Proc. Natl. Acad. Sci.*, **105**, 6439–6444. https://doi.org/10.1073/pnas.0802082105.